American Mineralogist, Volume 109, pages 1096–1105, 2024

Characteristics of congruent dissolution of silicate minerals enhanced by chelating ligand under ambient conditions

Jiajie Wang[1,†], Astin Nurdiana[1], Yoshinori Sato[1], Noriaki Watanabe[1], and Noriyoshi Tsuchiya[1,2,*]

[1]Department of Environmental Studies for Advanced Society, Graduate School of Environmental Studies, Tohoku University, Sendai 980-8579, Japan
[2]National Institute of Technology, Hachinohe College, Hachinohe 039-1192, Japan

Abstract

Natural and anthropogenic chelating ligands play important roles in promoting mineral dissolution during water-rock interactions. To address the remaining issue of how chelating ligands participate in the dissolution of minerals, this study investigated the dissolution characteristics of seven types of silicate minerals in the presence of a chelating ligand, *N,N*-bis(carboxymethyl)-L-glutamic acid (GLDA), which is a glutamic acid derivative, through batch dissolution experiments. The results showed that the dissolution of all types of silicate minerals, i.e., olivine (nesosilicate), epidote (sorosilicate), tourmaline (cyclosilicate), enstatite (single-chain inosilicate), hornblende (double-chain inosilicate), biotite (phyllosilicate), and anorthite (tectosilicate), can be enhanced by up to two orders of magnitude at both pH 4 and 8. The chelating ligand particularly facilitated the dissolution of minerals with a higher Al content, such as tourmaline and anorthite. Furthermore, the presence of chelating ligands enhanced the leaching of not only metals but also Si from minerals, resulting in a more congruent characteristic of mineral dissolution. A possible mechanism is that the chelating ligand adsorbs onto the negatively charged the mineral surface, which attracts more H^+ and polarizes Si-O and Mg-O bonds, thereby dissolving the minerals at a faster rate. These results have significant implications for understanding the dissolution of minerals in nature and for the application of chelating agents in geological and materials engineering.

Keywords: Chelating ligands, silicates, congruent, dissolution

Introduction

The dissolution of silicate minerals by geofluids is a fundamental chemical reaction in various natural systems on Earth, such as hydrothermal alteration, metamorphism, and weathering, which contribute to various geochemical phenomena, such as soil fertility, the global carbon cycle, reservoir porosities, cycling of metals, and formation of ore deposits (Konrad-Schmolke et al. 2018; Ribeiro et al. 2020; Cao et al. 2018; Li et al. 2018; Andreani et al. 2013). Recently, owing to the urgent need to mitigate climate change, the dissolution rates of Ca- and Mg-silicate minerals have received increasing attention because CO_2 can be stored as carbonate minerals after reaction with Ca and Mg ions, which is known as CO_2 mineralization (Ague and Nicolescu 2014; Wang et al. 2019).

Water-silicate mineral interactions have been extensively explored both experimentally and theoretically (Brantley 2008; Hamilton et al. 2001; Apollaro 2019; Lasaga and Lüttge 2004; Konrad-Schmolke et al. 2018; Putnis 2014) and have been divided into two basic types: congruent dissolution and incongruent dissolution (Green and Luttge 2006). In the natural environment, geofluids contain various dissolved components besides water molecules, including inorganic salts (Kikuchi et al. 2023; Kahl et al. 2022), gases such as O_2 and CO_2 (Kaszuba et al. 2013; Prigiobbe et al. 2009), and organic matter (Xu et al. 2017; Stumm 1997). These components are ubiquitous and play an important role in controlling the exchange of elements between the particle surface and solution. Natural and anthropogenic organic ligands can form coordinated covalent bonds with metal ions and play significant roles in promoting mineral dissolution (Ludwig et al. 1995; Huang and Keller 1970; Banfield et al. 1999; Neaman et al. 2006; Furrer and Stumm 1986). In nature, chelating organic ligands, usually with low molecular weight, such as various amino acids and siderophores; the latter can be abundantly secreted by organisms and assist in the extraction of Fe from the environment (Khan et al. 2018). Laboratory experiments have shown that Fe release and olivine [$(Mg,Fe)_2SiO_4$] dissolution can be enhanced by the formation of an Fe-ligand complex in the presence of the siderophore deferoxamine B (Torres et al. 2019; Takahashi et al. 2023).

Engineering technologies that apply chelating ligands to enhance mineral dissolution are also emerging. Chelating ligands, which selectively bind specific metal ions, have a great influence on the modification of mineral surfaces and are frequently used in ore-dressing processes, such as flotation, in the mining industry (Marabini et al. 2007). Watanabe et al. (2021) used *N,N*-bis(carboxymethyl)-L-glutamic acid (GLDA), a derivative of glutamic acid, to promote granite dissolution for developing methods for chemical stimulation of geothermal systems; they revealed a significant selective dissolution of the phyllosilicate biotite. They proposed a chelating ligand-assisted enhanced

* E-mail: noriyoshi.tsuchiya.e6@tohoku.ac.jp. Orcid 0000-0001-8176-6849
† Orcid 0000-0003-0469-5500

0003-004X/24/0005–1096$05.00/DOI: https://doi.org/10.2138/am-2023-9025

CO_2 mineralization process in which the preferred dissolution of the nesosilicate larnite was experimentally revealed (Wang et al. 2022). These observations underscore the significance and urgency of elucidating the considerable potential of chelating ligands in promoting mineral dissolution and understanding the underlying mechanisms of this promotion.

Many researchers have attributed the effects of ligands on dissolution to their ability to polarize and weaken the bond between the cation and the mineral lattice after adsorption onto the surface of minerals (Newcomb et al. 2017; Stumm and Wollast 1990; Park et al. 2003). Adsorption can be physical or chemical; the latter includes hydrophobic interactions, H-bonding, and water or cation bonding (Martin et al. 2014). Besides these direct effects, indirect effects have been suggested. For example, the decrease in free cation concentrations caused by ligand complexation in solution and the subsequent inhibition of recrystallization (i.e., precipitation) on mineral surfaces may enhance apparent mineral dissolution (Putnis et al. 1995). Moreover, it has also been reported that ligands, such as oxalate, can increase the solubility of quartz, indicating that chelating ligands may attack silicon tetrahedra as well as cations (Poulson et al. 1997). Therefore, in the presence of chelating ligands, mineral dissolution should be more congruent rather than incongruent. The latter often results in the formation of an inert silica-rich layer on the surface of the minerals (Liu et al. 2006). However, no evidence for the adsorption of oxalate on the quartz surface has been observed. Xiong et al. (2013) concluded that chelating ligands that directly combine with Si atoms to form covalent bonds are rare, except for specially prepared cyclic isocyanato(methyl)oligosiloxanes. Therefore, further experimental evidence is required to clarify the mechanism by which natural chelating ligands aid the dissolution of silicates.

Environmental conditions, such as temperature and pH, can influence the ability of a chelating ligand to bind ions and have been extensively studied (Wogelius and Walther 1992; Bradford et al. 2021; Onawole et al. 2019). Additionally, mineral dissolution behaviors and kinetics in chelating ligand solutions are potentially influenced by the silicate structure (Wang et al. 2021). Silicates with different connectedness of the silicate tetrahedra (Q) have different activation energies for the hydrolysis of Si-O bonds; the activation energy of the hydrolysis of a Si-O bond is considered to decrease with decreasing Q, i.e., more energy is required to dissolve a silicate with a higher Q (Gin et al. 2021). For instance, the preferred dissolution of biotite compared with plagioclase, K-feldspar, and quartz in granite is reported to be partially attributed to its lower Q value (Watanabe et al. 2021). Therefore, whether the preferential dissolution of some specific silicate minerals can be imposed by a chelating ligand remains unclear.

This study aims to gain a better understanding of the characteristics and mechanisms of overall silicate mineral dissolution in the presence of chelating ligands and to validate preferential dissolution through batch dissolution experiments. GLDA, a derivative of glutamic acid, which is an α-amino acid used by almost all living beings in the biosynthesis of proteins, was used to represent a general, widely available chelating ligand source for experiments. The dissolution behaviors of seven minerals belonging to the seven types of silicates, i.e., nesosilicates, sorosilicates, cyclosilicates, single-chain inosilicates, double-chain inosilicates, phyllosilicates, and tectosilicates, were investigated in ambient systems with GLDA. Following that, our focus was on olivine (a nesosilicate, the simplest of the silicates), aiming for a more straightforward investigation into the mechanism through which chelating ligands facilitate the dissolution of silicates via mineral surface chemical analysis. This study also aimed to contribute to the development of chelating ligand-assisted engineering technologies.

Methodology

Materials

A 40 wt% GLDA tetrasodium salt (Na_4GLDA) solution with a pH of 13.8 was purchased from Tokyo Chemical Industry, Japan. The initial molar concentration of Na_4GLDA solution was calculated to be ~1.3 mol/L based on the weight fraction, and the density was determined by weighing the Na_4GLDA solution in a given volume. GLDA solutions with the desired concentrations and pH values were prepared by diluting the initial Na_4GLDA solution with Milli-Q water and adjusting the solution pH using concentrated (60.0–61.0%) nitric acid (HNO_3) from Kanto Chemical, Japan.

Seven representative minerals of silicates were selected for the experiments: olivine (nesosilicate), epidote (sorosilicate), tourmaline (cyclosilicate), enstatite (single-chain inosilicate), hornblende (double-chain inosilicate), biotite (phyllosilicate), and anorthite (tectosilicate). The general formulas of all the minerals are listed in Table 1. Olivine particles were obtained from Damaping, China; epidote from the Trinidad Valley in Baja California, Mexico; tourmaline from Fukushima, Japan; enstatite from Tanzania; biotite from Nellore, India; and anorthite from Otaru, Hokkaido, all of which were purchased from Nichika Inc., Japan. Hornblende was handpicked from gneiss collected from the Sør Rondane Mountains of East Antarctica. The purity of these minerals was checked through X-ray diffraction (XRD, Rigaku, ZSX Primus IV) with Cu*K*α radiation to confirm significant peaks of impurities were not present in the patterns. Furthermore, major elemental compositions of the minerals were obtained using an electron probe microanalyzer (EPMA, JEOL JXA-8200) at Tohoku University, Japan, as shown in Table 2. Quantitative analysis of the major minerals was conducted at an accelerating voltage of 15 kV and a beam current of 12 nA.

The mineral grains were ground and sieved to obtain a size of <300 μm for the experiments. Owing to the relatively large size of the mineral particles, their specific surface area (SSA) was difficult to determine by Brunauer-Emmett-Teller (BET) techniques, which determine SSA ranging from 1–1000 m^2/g. Instead, the particle size distributions of the mineral powders were first analyzed using a particle size analyzer (MASTERSIZER 3000, Malvern Panalytical Ltd., U.K.), and then the SSA was calculated by assuming that the particles were spherical (expect biotite, which is known as layered mineral). The olivine, epidote, tourmaline, enstatite, hornblende and anorthite powders used in the experiments exhibited calculated SSAs of 0.13, 0.60, 0.46, 0.6, 0.78, and 0.24 m^2/g, respectively. The SSA estimation of biotite, a layered mineral, is not applicable using the same method. Instead, the average specific surface area (SSA_{BET}) of biotite was calculated based on particle size distributions. Bray et al. (2015) specifically determined that the SSA_{BET} of biotite particles in the size ranges of 25–53, 53–180, and 180–300 μm were 3.25, 0.92, and 0.64 m^2/g, respectively. Given that the fraction of biotite particles used in this study in these ranges comprised 47.1, 41.6, and 11.9%, respectively, the calculated average SSA_{BET} of biotite is 1.97 m^2/g. Although the above assumptions will underestimate the SSA, it will not affect the investigation of the GLDA's effects because the same minerals were used in the experiments.

Dissolution experiments using a broad range of silicates

Initially, the dissolution characteristics of seven types of silicate minerals in the presence of GLDA were examined through batch dissolution experiments

Table 1. Minerals used in dissolution experiments

Silicate type	Q	Mineral	General formular
Nesosilicate	0	Olivine	$(Mg,Fe)_2SiO_4$
Sorosilicate	1	Epidote	$Ca_2(Al_2Fe)(SiO_4)(Si_2O_7)O(OH)$
Cyclosilicate	2	Tourmaline	$(Ca,K,Na)(Al,Fe,Mg,Mn)_3$ $(Al,Fe)_6(BO_3)_3(Si,Al)_6O_{18}(OH)_4$
Inosilicate: single-chain	2	Enstatite	$MgSiO_3$
Inosilicate: double-chain	2,3	Hornblende	$(Ca,Na)_2(Mg,Fe,Al)_5(Al,Si)_8O_{22}(OH)_2$
Phyllosilicates	3	Biotite	$K(Mg,Fe)_3AlSi_3O_{10}(OH)_2$
Tectosilicates	4	Anorthite	$(Ca,Na)Al_2Si_2O_8$

Note: Q is the number of bridging O atoms (connectivity or connectedness) of the Si atoms.

Table 2. Averaged result of chemicals (mass%) from electron probe microanalysis and calculated mineral formulas

	Olivine	Epidote	Tourmaline	Enstatite	Hornblende	Biotite	Anorthite
SiO_2	40.77	33.72	34.25	44.60	49.29	32.41	43.95
TiO_2	N.D.	0.10	0.24	1.06	0.17	1.83	N.D.
Al_2O_3	0.01	20.41	33.88	15.26	4.04	18.20	34.95
FeO	8.68	13.77	11.76	0.36	11.57	30.31	0.53
MnO	0.13	0.22	0.16	N.D.	0.22	0.21	0.06
MgO	50.23	1.49	1.80	18.87	17.23	4.61	0.12
CaO	0.06	21.97	0.17	12.18	12.61	N.D.	19.34
Na_2O	N.D.	0.37	1.88	2.84	0.74	0.57	0.42
K_2O	N.D.	N.D.	0.03	1.84	0.19	8.04	0.01
B_2O_3	N.D.	N.D.	8.23	N.D.	N.D.	N.D.	N.D.
Total	99.88	91.91	92.40	97.00	96.06	96.22	99.38
No. of oxygen	4	12.5	31	6	23	11	8
Si^{4+}	1.00	2.98	5.85	1.64	7.27	2.59	2.05
Ti^{4+}	–	–	0.03	0.03	0.02	0.10	–
Al^{3+}	–	2.13	6.82	0.66	0.70	1.71	1.92
Fe^{3+}	0.18	1.01	1.68	0.01	1.07	2.02	0.02
Fe^{2+}	–	–	–	–	0.34	–	–
Mn^{2+}	–	0.01	0.02	–	0.03	0.01	–
Mg^{2+}	1.82	0.20	0.46	1.03	3.80	0.55	0.01
Ca^{2+}	–	2.08	0.03	0.48	1.99	–	0.97
Na^{+}	–	0.06	0.62	0.20	0.21	0.08	0.04
K^{+}	–	–	–	0.08	0.03	0.82	–
B^{3+}	–	–	3.00	–	–	–	–
Al[T]	–	0	0.15	0.36	0.70	1.41	1.92
Al[T]/Al	–	0	0.02	0.55	1.00	0.82	1.00

Notes: N.D. indicates the concentration lies before the detection limit. Al[T] refers to the Al that substituted Si in the tetrahedra, and Al[T]/Al refers to the ratio of Al on the Si side.

utilizing mineral powders and analyzing changes in solution chemistry. The 20 g/L mineral dissolution batch experiments were performed in a shaker machine by reacting 1.6 g of mineral powders with 80 mL Milli-Q water or 2 wt% GLDA solution (0.065 mol/L) in 100 mL plastic bottles. The initial pH of the GLDA solution was regulated to 4 and 8, and the dissolution experiments were conducted at ambient temperature (20 °C) for 120 min at a shaking speed of 120 rpm. During the experiments, a small amount of a solution sample (1 mL) was intermittently sampled using a syringe via filtering with a 0.45 μm syringe filter. Five samples, each consisting of 1 mL, were extracted at various points during each experiment. The reduction in volume was within 7% of the total initial solution (80 mL); therefore, it is anticipated that the sampling process will not significantly impact the dissolution results. After the reaction, the solution and solid in the beaker were collected separately using a membrane filter with an average pore diameter of 0.45 μm. With the exception of sodium (Na), the initial elemental concentration in the 1% GLDA solution is considered negligible. Blank experiments were conducted by performing dissolution experiments of the same mineral in Milli-Q water at both pH 4 and 8.

The solution samples were analyzed for their pH and elemental concentrations (including free cations and those combined with GLDA) via inductively coupled plasma-optical emission spectrometry (ICP-OES; Agilent 5100). The measurements were conducted three times and showed good reproducibility within an error margin of 3%. Standard deviation values were not calculated in this study but were expected to be low based on the measurements. The element extraction ratio was calculated by dividing the element concentration in the extraction solution by the initial element composition (mass%) of the mineral and the starting reactor mineral concentration (20 g/L).

The mineral dissolution rate, in mol/m^2/s, was calculated by dividing the Si extraction (mmol/L) by the mineral concentration (20 g/L), reaction time (120 min), and mineral SSA (m^2/g), assuming that the reaction was of zero-order. Note that this assumption is only used to assess the ability of GLDA and does not represent the real dissolution kinetics. To discuss the characteristics of silicate dissolution, a dissolution factor (α) was introduced and calculated as follows (Eqs. 1 and 2):

$$\alpha = \beta_{solution}/\beta_{mineral} \quad (1)$$

$$\beta = [M]/[S] \quad (2)$$

where [M] refers to the sum of the molar concentrations of the main metals, i.e., Mg, Fe, Ca, and Mn (Mg, Fe, Ca, Mn, and Al in the case of tourmaline and enstatite), in the extraction solutions or in the initial minerals, and [S] refers to the molar concentrations of Si (Si plus Al in the case of hornblende, biotite, and anorthite). The calculation of Al was simplified according to the measurement results listed in Table 2. B is the ratio of main metals to Si (including Al that replaced Si) in the solution or in minerals. If $\alpha > 1$, the main metals dissolve faster than Si (including Al that replaced Si), while if $\alpha < 1$, Si (including Al that replaced Si) dissolves faster than the main metals. Both of these situations suggest an incongruent dissolution and result in the formation of a silica layer, here called an apparent leaching layer. When α approaches 1, dissolution is considered more congruent.

Dissolution enhancement mechanism investigation using olivine

To investigate the mechanisms of mineral dissolution in chelating ligand solutions, the surface chemistry of olivine particles was characterized before and after dissolution in a 2 wt% GLDA solution for 2 h. Nesosilicates are, in some ways, the simplest of silicates, with a basic structure of an isolated Si tetrahedron surrounded by cations. Therefore, while this study encompasses a broad range of silicates, concentrating on olivine (nesosilicates) facilitated the most straightforward examination of the interactions between ligands and minerals.

First, X-ray photoelectron spectroscopy (XPS) was used to identify the mineral surface chemicals (within 10 nm). Relatively large olivine particles were picked from the solid sample that had reacted with the GLDA solution and washed with Milli-Q water several times in an ultrasonic cleaning tank to remove the potential leaching layer or GLDA layer and uncover the fresh reacted surface layer, followed by drying at 60 °C in an oven for 24 h for XPS measurement. The XPS measurement was carried out on a K-Alpha XPS system (ThermoFisher Scientific Inc., U.S.A.) equipped with a monochromatic Al$K\alpha$ source. The vacuum pressure during the analysis was $<2 \times 10^{-8}$ mbar, and carbon C 1*s* line with a position at 284.8 eV) was used as a reference for charging effect correction.

The residual olivine particles collected after reaction with the GLDA solution were dried directly to maintain the true composition of the mineral surface layer during dissolution. Representative particles of suitable size were selected and cut from two sides using a focused ion beam (FIB) to produce rectangular craters and a lamella in the middle, having a thickness, width, and depth of approximately 0.5, 12, and 10 μm, respectively, from the surface. The surface of the lamella was covered with amorphous carbon as a buffer layer, and tungsten (W) was continuously deposited to prevent damage to the mineral surface by the ion beam. The surface morphologies of the prepared specimens were analyzed using scanning electron microscopy (SEM; SU-8000, Hitachi, Japan), and the chemical compositions were analyzed as a function of depth using EPMA. Elemental mapping analysis of the major minerals was conducted at an accelerating voltage of 15 kV and a beam current of 120 nA with a pixel size and a dwell time of 0.15 μm and 100 ms, respectively.

Results and discussion

Mineral dissolution characteristics in chelating ligand solutions

The addition of GLDA significantly enhanced the dissolution of all mineral types within 120 min at both pH 4 and 8. Figure 1 illustrates the changes in fluid chemistry over time during the dissolution of olivine in Milli-Q water (Figs. 1a and 1c) and the GLDA solution (Figs. 1b and 1d). In GLDA solution with an initial pH of 4, Mg and Si concentrations reached 4.6 and 2.8 mmol/L, respectively; both were 14 times higher than that in water with the same pH of 4. In water, olivine dissolution was initiated by an H^+ attack on the metals in the lattice, whereas in the GLDA solution, olivine dissolution was stimulated by both H^+ and GLDA attacks. Furthermore, mineral dissolution in the GLDA solutions continued for up to 120 min and showed a tendency to increase further (Figs. 1b and 1d), indicating the suppression of an inactive production layer formation. The possible reaction between olivine and the GLDA solution is shown in Equations 3 and 4:

$$Mg_2SiO_4 + 2GLDA^{4+} + 4H^+ \rightarrow 2Mg\text{-}GLDA^{4+} + H_4SiO_4 \quad (3)$$

$$Mg_2SiO_4 + 4H^+ \rightarrow 2Mg^{2+} + H_4SiO_4 \quad (4)$$

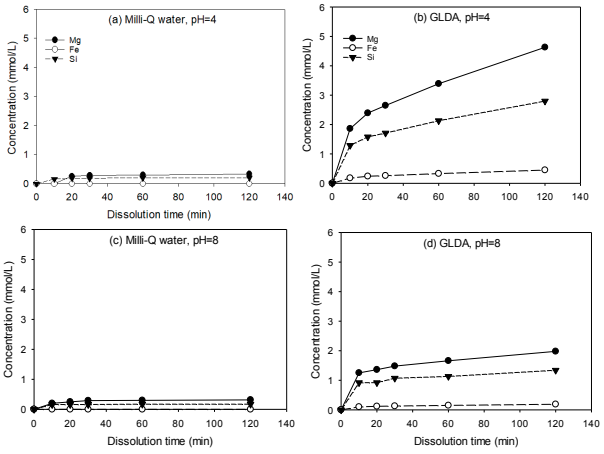

Figure 1. Mg, Fe, and Si concentration changes as a function of time during olivine dissolution in (**a**) Milli-Q water at pH 4, (**b**) *N,N*-bis(carboxymethyl)-L-glutamic acid (GLDA) solution at pH 4, (**c**) Milli-Q water at pH 8, and (**d**) GLDA solution at pH 8.

The Si extraction ratios for all experiments are presented in Figure 2a to describe the extent of the dissolution of silicate minerals. Notably, Si extraction in the GLDA solution was significantly higher than that in water for all minerals, with biotite mixed with the GLDA solution at an initial pH of 4 exhibiting the highest amount of Si extraction, partly due to its higher SSA. Mineral dissolution rates, expressed in units of mol/m^2/s, were also calculated using the extracted Si concentrations and are summarized in Figure 2b and Table 3. The dissolution rates of minerals in both the GLDA solution and Milli-Q water were generally faster at pH 4 than at pH 8, consistent with previous studies (e.g., Hänchen et al. 2006), hornblende being the exception. Mineral dissolution was enhanced by up to two orders of magnitude in the GLDA solutions and varied depending on the type of silicate mineral. This leads to a change in the mineral dissolution preference, even at the same pH value. For example, hornblende dissolved faster than anorthite in Milli-Q water with a pH of 4, whereas the opposite was observed in a GLDA solution at the same pH. However, the mineral dissolution rate in the GLDA solution was not correlated with the number of bridging O atoms to Si atoms (Q) for the minerals studied in both Milli-Q water and the GLDA solution. It should be noted that phyllosilicate dissolution can be more complex than other silicates, and environmental pH can change the dissolution preference of minerals; these kinds of changes may also be induced by the chelating ligands present in the environment.

To evaluate the ability of the GLDA to enhance the dissolution of silicate minerals, an enhancement factor was introduced. This factor was defined as the ratio of Si extracted in the GLDA solution to that in Milli-Q water at the same pH value. The results of this calculation are presented in Table 3. Except for epidote and enstatite, the dissolution of all the minerals was enhanced by a greater factor at pH 4 than at pH 8. The dissolution of tourmaline (cyclosilicates) and anorthite (tectosilicates) was the most substantially enhanced, with an enhancement factor exceeding 200 in the GLDA solution at pH 4, whereas the enhancement factor of hornblende dissolution was relatively small. These results

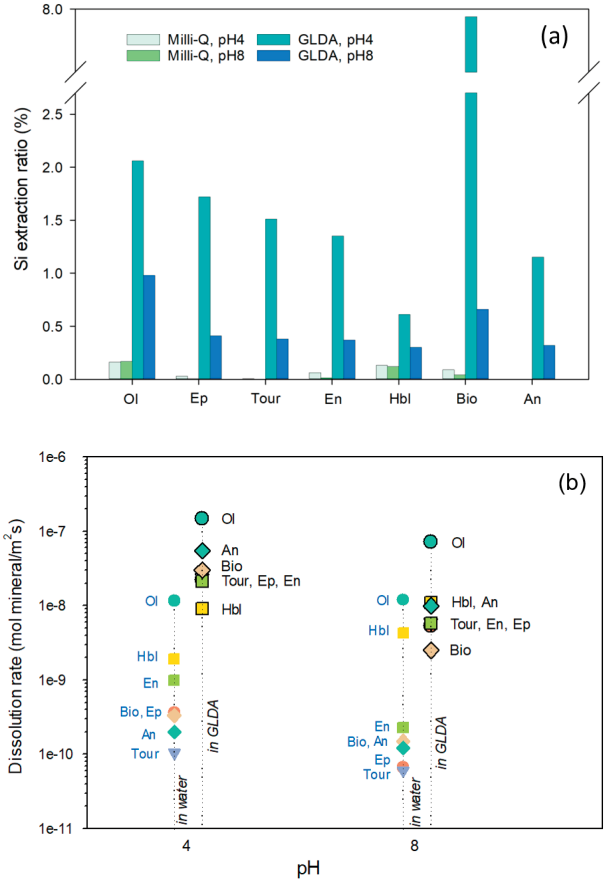

Figure 2. (**a**) Si extraction ratio from minerals after dissolving in Milli-Q water and *N,N*-bis(carboxymethyl)-L-glutamic acid (GLDA) solution at pH 4 and 8 for 120 min, (**b**) dissolution rate of minerals in Milli-Q water (points without edge color) and GLDA solution (points without black edge color) at pH 4 and 8 for 120 min. Ol = olivine; Ep = epidote; Tour = tourmaline; En = enstatite; Hbl = hornblende; Bio = biotite; An = anorthite.

suggest that chelating ligands can effectively enhance the dissolution of silicate minerals, with different minerals exhibiting varying degrees of enhancement.

The correlation between the enhancement factor and the fractions of Si and Al in the minerals and the value of Q is shown in Figure 3. Generally, the enhancement factor exhibited a weak negative correlation with the Si fraction in the minerals

Table 3. Mineral dissolution rate and enhancement factor in *N,N*-bis(carboxymethyl)-L-glutamic acid (GLDA) solution compared with that in Milli-Q water

Mineral	Dissolution rate in GLDA solution (mol/m^{2}s)		Dissolution rate in Milli-Q water (mol/m^{2}s)		Enhancement factor	
	pH 4	pH 8	pH 4	pH 8	pH 4	pH 8
Olivine	1.5×10^{-7}	7.2×10^{-8}	1.2×10^{-8}	1.2×10^{-8}	12.7	5.90
Epidote	2.2×10^{-8}	5.3×10^{-9}	3.7×10^{-10}	6.8×10^{-11}	60.1	78.2
Tourmaline	2.3×10^{-8}	5.9×10^{-9}	1.0×10^{-10}	6.1×10^{-11}	222	96.4
Enstatite	2.1×10^{-8}	5.8×10^{-9}	9.9×10^{-10}	2.3×10^{-10}	21.3	25.0
Hornblende	9.0×10^{-9}	1.1×10^{-8}	2.0×10^{-9}	4.4×10^{-9}	4.60	2.50
Biotite	3.0×10^{-8}	2.5×10^{-9}	3.4×10^{-10}	1.5×10^{-10}	89.4	16.5
Anorthite	5.5×10^{-8}	9.9×10^{-9}	2.0×10^{-10}	1.2×10^{-10}	269	80.7

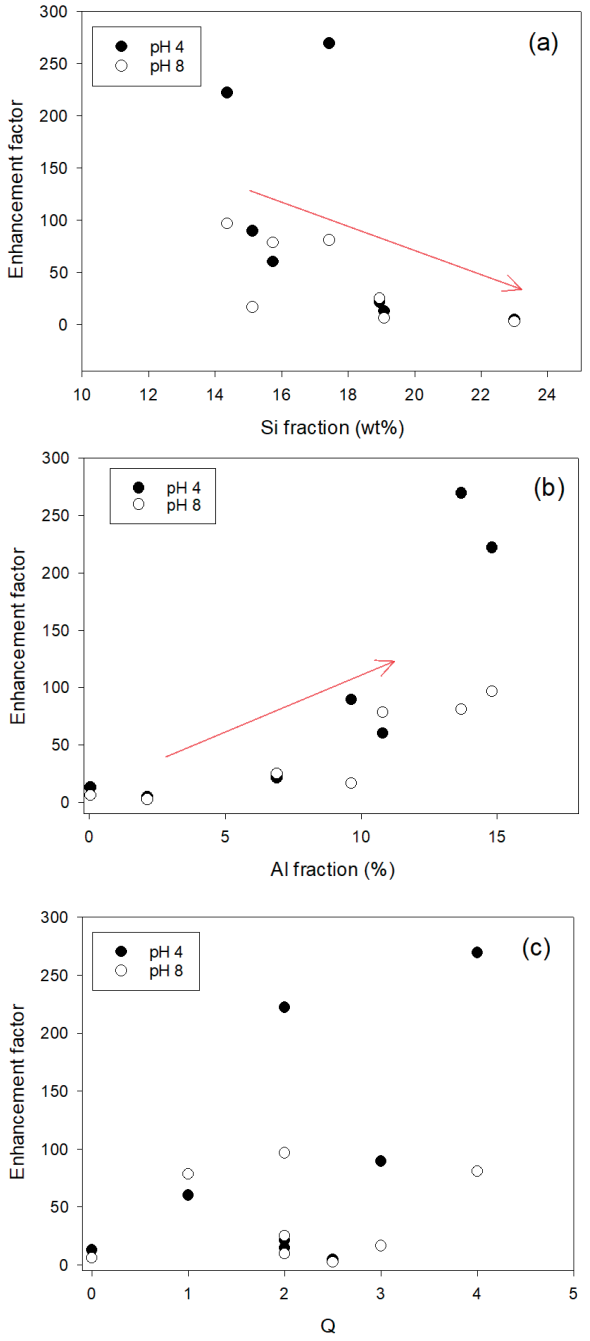

Figure 3. Relationships between enhancement factor and (**a**) Si fraction, (**b**) Al fraction, and (**c**) number of bridging O atoms with Si atoms, Q.

(Fig. 3a) but a positive correlation with the Al fractions (Fig. 3b), particularly at pH 8. The chelate stability constant was expected to be higher at neutral to alkaline pH than at acidic pH. Chelating ligands, including the GLDA utilized in this investigation, usually exhibit a strong affinity for Al, while their affinity for Si is deemed unlikely (Kołodyńska 2011). Therefore, minerals with higher Al contents, regardless of the Al position in the mineral lattice, are more reactive with chelating ligands, explaining the positive correlation between the enhancement factor and the Al fraction. Moreover, while the activation energy of Si-O bond hydrolysis is purported to decrease with decreasing polymerization of the silicate tetrahedra, represented by Q, the experimental results of this study did not establish a definitive correlation between the enhancement factor and Q (Fig. 3c). For example, tourmaline and enstatite, although having the same Q value of 2, display different enhancement factors. Consequently, the activation energy of Si-O bond hydrolysis is not the primary factor governing the dissolution selectivity of silicate minerals in chelating ligand solutions.

The dissolution factor, α, was calculated to investigate the dissolution characteristics of silicate minerals. As shown in Figure 4. At both pH 4 and 8, all minerals showed lower α values and the α values were closer to 1 in GLDA solution than in Milli-Q water, indicating that the extraction of Si and Al was enhanced more than other metals and the dissolution is more congruent. Significant decreases in the values of α were observed in the GLDA solutions for epidote, tourmaline, enstatite, and anorthite at pH 4 (Fig. 4a) and for epidote and anorthite at pH 8 (Fig. 4b). This more congruent dissolution in the GLDA solution may suppress the formation of a Si-rich layer and result in prolonged dissolution, which is consistent with the solution chemistry measurements shown in Figure 1.

Dissolution mechanism of minerals represented by olivine-GLDA reaction

To have the easiest investigation into the reaction processes between ligands and minerals, olivine (nesosilicates) was chosen as a representative of a diverse range of silicates. Olivine particles before and after the reaction in the GLDA solution (initial pH of 4) were analyzed by XRD to further explore the dissolution mechanisms. The relative intensity was determined by dividing the absolute intensity of each peak by the absolute intensity of the most intense peak, i.e., the (130) diffraction peak, when comparing the raw olivine and olivine that reacted with the GLDA solution and the (112) diffraction peak when comparing the original olivine and olivine that reacted in water. The results presented in Figure 5 indicate that olivine dissolution occurred on the surface of the crystals in the GLDA solution. Crystal surfaces such as (020), (021), (131), and (015) were extensively dissolved, whereas (130), (210), and (211) surfaces were relatively less susceptible to dissolution. The dissolution of olivine in GLDA and water might have occurred on different crystal surfaces. For example, the dissolution of surfaces (020), (131), and (112) in the GLDA solution was faster than that in water. These findings suggest that the presence of chelating ligands changes the dissolution preference for silicate minerals and influences the preferred dissolution surfaces of the mineral crystals. However, the factors controlling the selective crystal surface for the dissolution of chelating ligands must be further explored.

The surface chemistry and composition of the olivine particles were analyzed through XPS, both before and after the reaction with the GLDA solution, to investigate the dissolution mechanisms of minerals within a depth of 10 nm from the surface. Prior to the measurement, the reacted olivine particles were washed several times with water to remove any possible leaching layers. A full survey scan (Fig. 6) reveals the presence of Mg, Fe, Si, O,

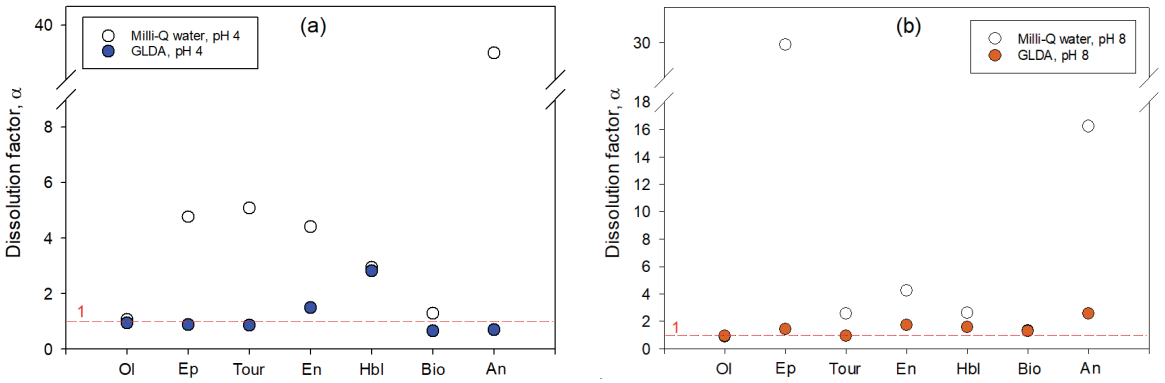

Figure 4. Dissolution factor (α) calculated from mineral dissolution in Milli-Q water and *N,N*-bis(carboxymethyl)-L-glutamic acid (GLDA) at (**a**) pH 4 and (**b**) pH 8 for 120 min. Red dashed line shows the values of 1, when the dissolution is congruent.

and C in the sample. The intensity was normalized by dividing the absolute intensity by the absolute intensity of the C 1*s*. The detected carbon was considered to originate from impurities in the olivine organic matter. No considerable difference was observed in the elemental peaks before and after the reaction, except for the Na peak after the reaction, indicating the adsorption of GLDA-4Na onto the olivine surface.

The narrow-range Si 2*p*, O 1*s*, and Mg 1*s* spectra of olivine before and after the reaction are illustrated in Figure 6, revealing a slight shift in the binding energy to a lower position for all three elements. As previously suggested, the decreased energy for Si 2*p* is related to the negatively charged silica tetrahedra (Seyama and Soma 1985). Additionally, Zhu et al. (2018) and Morrow et al. (2014) described different silicon dissolution mechanisms under acidic and alkaline conditions, with a shift in the binding energies of O 1*s* and Si 2*p* to a lower position attributed to the formation of surface sites for SiO^- in an alkaline solution, whereas the shift to a higher position in acid solutions corresponds to the formation of surface sites for $SiOH_2^+$. Therefore, the mineral surfaces that reacted with GLDA at pH 4 were negatively charged, probably due to the adsorption of negatively charged $GLDA^{4-}$. Notably, the point of zero charge for olivine is higher than 8, for example 9.85, as suggested by (de Souza et al. 2013); thus, a positively charged surface was expected under acidic conditions, which is inconsistent with that in the GLDA solution. This type of negatively charged surface in the GLDA solution may directly polarize the chemical bonds between metals or Si and O in the mineral lattice or indirectly enhance the dissolution of minerals by attracting more H^+; thereby enhancing the dissolution of not only metals but also Si in the GLDA solution.

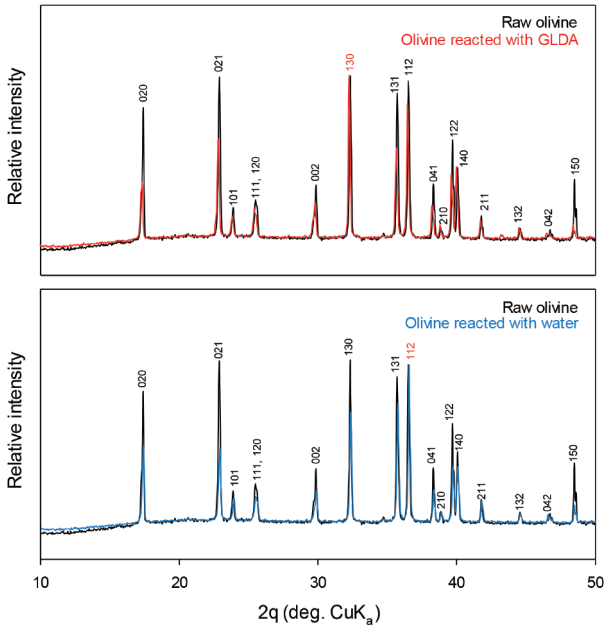

Figure 5. X-ray diffraction (XRD) patterns of olivine after reacting with *N,N*-bis(carboxymethyl)-L-glutamic acid (GLDA) solution (top) and water (bottom). XRD patterns of raw olivine and olivine after reacting with GLDA solution (pH 4), relative intensities are shown by diving the absolute intensity of every peak by the absolute intensity of the highest intensity peak: (130) diffraction peak when comparing the raw olivine and olivine reacted with GLDA solution and (112) diffraction peak when comparing the raw olivine and olivine reacted in water.

Olivine particles collected after reaction with the GLDA solution were also cut with a FIB from the surface to obtain a thin slice of the sample and analyzed using SEM and EPMA to investigate the elemental distributions near the mineral surface and the reaction of GLDA with the olivine surface. The shape of the particle segment cut by the FIB is shown in Figure 7. The FIB-treated part for observation was approximately 10 μm in depth and 0.5 μm in thickness (not shown in the figure), with the surface of the segment being covered by W and C to increase its strength. As shown in Figure 7b, many fine particles (<1 μm) were observed on the surface of the reacted olivine (for example, on the right side of the figure), which were amorphous silica.

Elemental mapping of a thin slice of olivine was analyzed using EPMA to investigate the changes in elemental distribution with distance from the surface, as depicted in the red box of Figure 8. However, the elemental distribution data outside the red box cannot be used for comparison because of the larger thickness of the segment and non-flat surface. The results show that Mg, Fe, and Si exhibited different distributions. Specifically, the distribution of Mg was depleted on the surface of the olivine, with the composition decreasing as depth (i.e., distance from the surface)

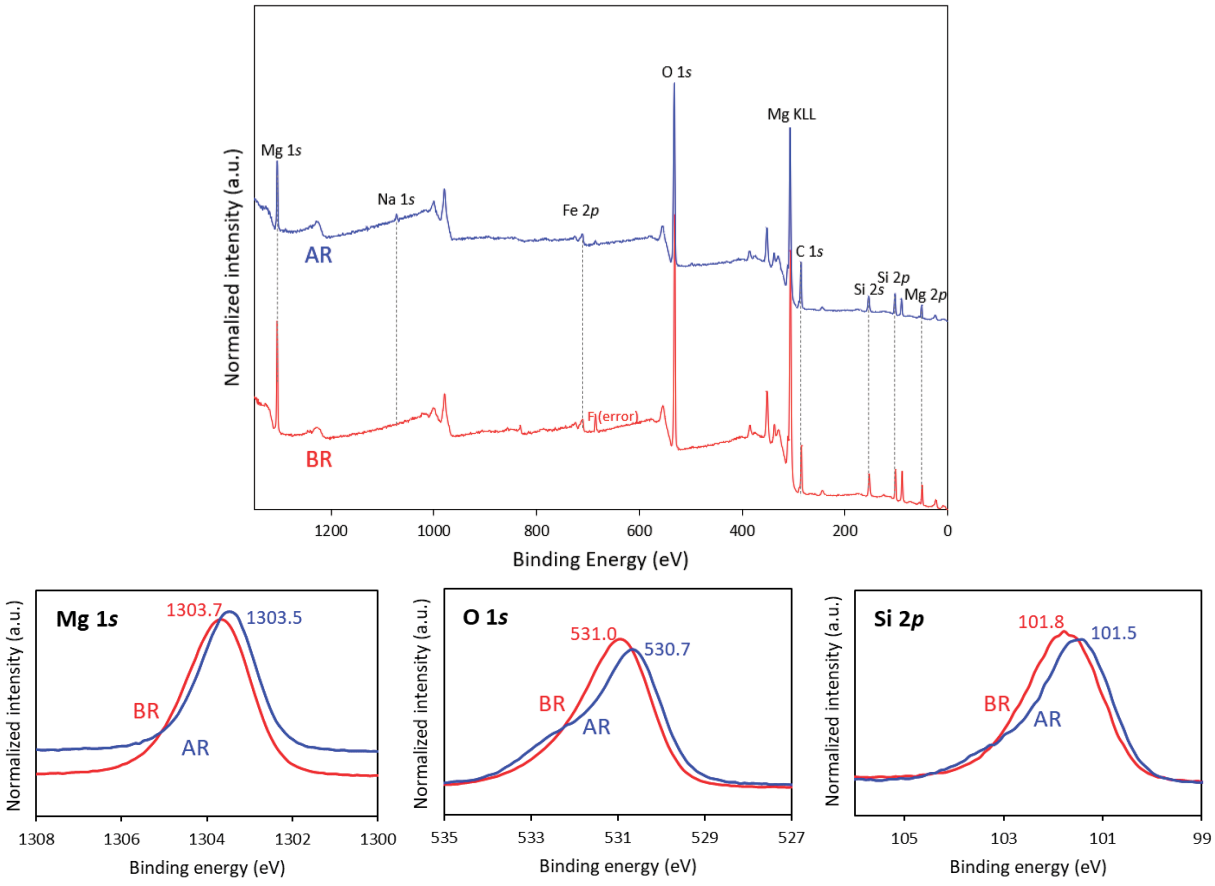

Figure 6. X-ray photoelectron spectroscopic (XPS) survey spectra and XPS narrow-range spectra of the Si 2*p*, O 1*s*, and Mg 1*s* of olivine before and after reaction with GLDA solutions. BR: before reaction, AR: after reaction.

increased up to 3–5 μm. In the same area, Si exhibited a different distribution: it was concentrated in some areas near the surface, such as the upper-right side of the Si mapping in Figure 8, whereas some inner spaces were severely depleted, with Si concentrations similar to those in the blank sites. One possible explanation for this is that the hollowing-out-from-within dissolution phenomenon may be attributed to the irregular surface of the initial olivine, with the lower left part recessed at the beginning and the upper right part raised. Possibly, GLDA entered the olivine particle from the initial recessed part, leading to the removal of Si from the lattice due to GLDA attack, while Mg combined with GLDA and partially remained near the surface. However, this GLDA-Mg layer can be easily removed by washing or during the reaction due to friction between particles under stirring. The distribution of Fe, on the other hand, was found to be evenly distributed throughout the thin slice to a depth of 10 μm. Furthermore, the EPMA elemental mapping results support the XPS observation that both the Si and Mg bonds with O may be attacked by the GLDA molecules.

By combining the olivine dissolution experimental results and surface chemical analyses, a potential mechanism for the chelating ligand-promoted dissolution of silicate minerals is depicted in Figure 9. Upon contact with a mineral surface, a chelating ligand can be physically or chemically adsorbed (Nowack 2002). Through chemical adsorption, chelating ligands form stable coordination complexes with metal ions, the metal-O bonds are polarized, and they become more susceptible to breakage. This breakage promotes the dissolution of SiO_2, resulting in the release of H_4SiO_4 tetrahedra. The XPS data demonstrate that the adsorption of chelating ligands on the mineral lattice rendered it negatively charged, thereby attracting more protons for the reaction. The EPMA elemental distribution results suggest that Si was depleted from relatively deep areas of olivine during dissolution. We hypothesize that this is due to the release of SiO_4 tetrahedra from the lattice and formation of $H_4SiO_4^0$ in solution, while chelating ligands bound to metals are still negatively charged and, therefore, detach slowly from the mineral surface. However, speculation regarding the interaction between Si and chelating ligands requires further scientific verification. It is important to note that, for simplicity, olivine (a nesosilicate mineral) was used in the mechanism investigation; however, the dissolution of other minerals, especially biotite (phyllosilicate), would be much more complex.

Implications

Water-rock interactions can be significantly influenced by the presence of chelating ligands, and this study highlights that the structure and composition of silicate minerals significantly affect their dissolution in the presence of chelating ligands, besides environmental conditions such as pH and temperature

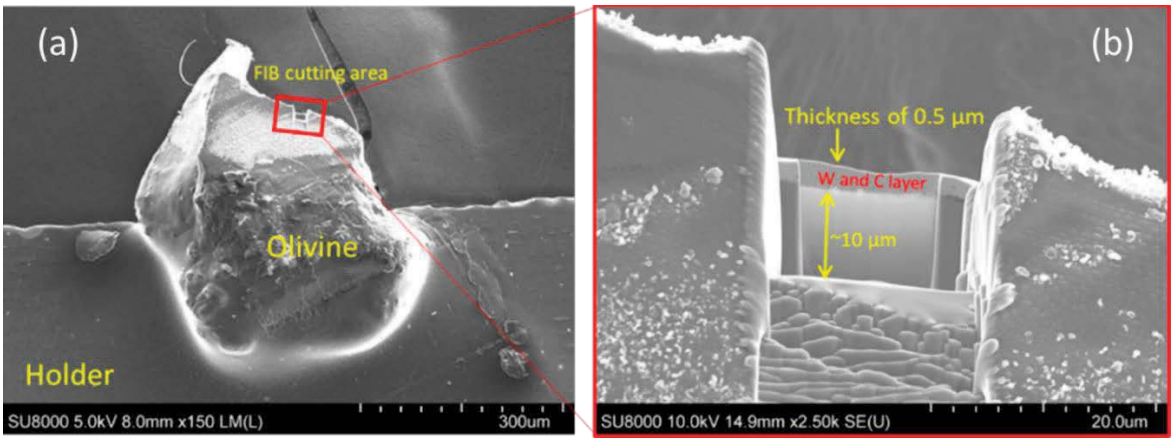

Figure 7. (**a**) Scanning electron microscopic (SEM) image of reacted olivine segment cut with focused ion beam (FIB). (**b**) Magnified SEM image of the cut olivine segment in the red box in **a**.

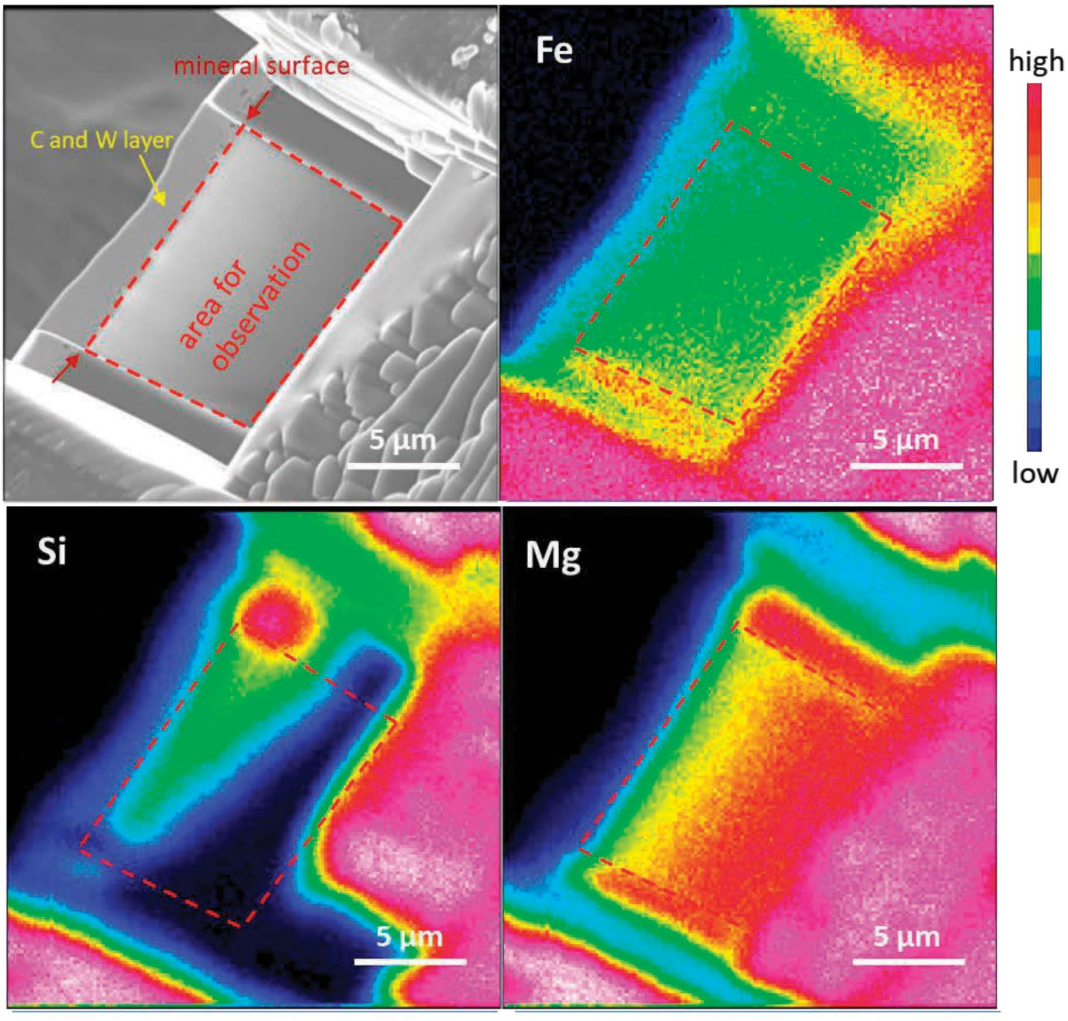

Figure 8. Electron probe microanalysis (EPMA) elementary mapping of the reacted olivine segment cut with focused ion beam (FIB).

(Walter et al. 2019; Yadav and Chakrapani 2006). Specifically, cyclosilicate tourmaline and tectosilicate anorthite are more easily accelerated in the presence of chelating ligands, possibly because of their relatively high-Al content, regardless of their position in the mineral lattice. Notably, this type of dissolution promotion may be observed with other chelating ligands that possess similar adsorption properties and chemical bond polarizations. Consequently, the preference for mineral dissolution varies more in the presence of chelating ligands than in the presence of water, suggesting a different mineral dissolution rate and preference in the natural environment than what has been predicted for the water system.

Furthermore, it was confirmed that all types of silicate minerals display relatively congruent dissolution characteristics in the presence of a derivative of natural chelating agents because the dissolution of metals, as well as silicon, was enhanced. This congruent dissolution of minerals in the chelating agent solution can be sustained for a relatively long time. Based on chemical analysis of the mineral surface after dissolution, a potential mechanism for the promotion of silicate mineral dissolution by chelating ligands is proposed in this study. Negatively charged chelating agents may first be adsorbed on the surface of minerals in an aqueous solution, polarizing Si-O and Mg-O bonds. Simultaneously, such adsorption attracts more H^+ from the solution for the reaction. Thus, by reducing the pH in the presence of chelating agents, a more effective increase in the dissolution rate of minerals was obtained compared with that without chelating agents. The separated SiO_2 may preferentially leave the mineral surface before the metal ions rather than the chelating agents bound to the metal ions, possibly because of their negative charge.

Overall, this work significantly enhances our understanding of mineral dissolution behaviors in fluids containing chelating ligands in the natural environment and potentially contributes to the development of chelating ligand-assisted engineering technologies for geothermal exploration and CO_2 mineralization, which typically target rocks containing various silicate minerals, such as basalt and granite. Further studies are required to explore the underlying chelating ligands and Si interaction mechanisms in greater detail.

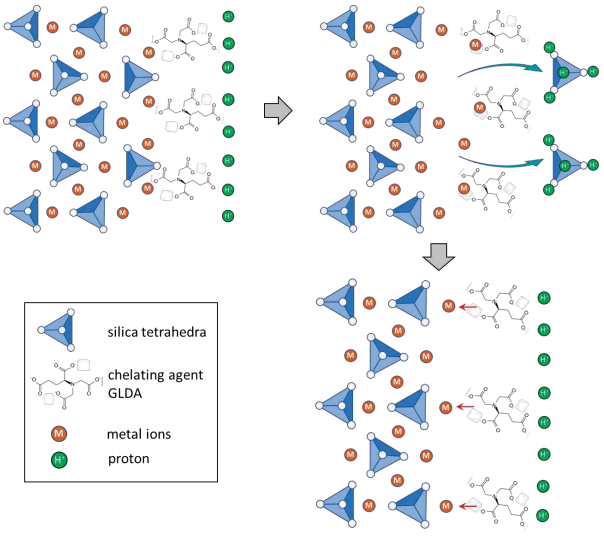

Figure 9. Potential mechanism of chelating ligand-promoted dissolution of olivine, using *N,N*-bis(carboxymethyl)-L-glutamic acid (GLDA) as a representative chelating ligand.

Acknowledgments and Funding

This study was partially supported by the Japan Society for the Promotion of Science (JSPS) through a Grant-in-Aid for Early-Career Scientists (No. 21K14571), Grants-in-Aid for Scientific Research (A) (No. 21H04937), Grants-in-Aid for Scientific Research (B) (No. 22H02015), Challenging Research (Pioneering) (No. 21K18200), Grants-in-Aid for Scientific Research (S) (No. 22H04932) and JST/JICA SATREPS (No. JPMJSA1703). We thank Kenichi Motomiya of Tohoku University for FIB sample preparation.

References Cited

Ague, J.J. and Nicolescu, S. (2014) Carbon dioxide released from subduction zones by fluid-mediated reactions. Nature Geoscience, 7, 355–360, https://doi.org/10.1038/ngeo2143.

Andreani, M., Daniel, I., and Pollet-Villard, M. (2013) Aluminum speeds up the hydrothermal alteration of olivine. American Mineralogist, 98, 1738–1744, https://doi.org/10.2138/am.2013.4469.

Apollaro, C. (2019) Geochemical modeling of water-rock interaction in the granulite rocks of lower crust in the Serre Massif (Southern Calabria, Italy). Geofluids, 2019, e5602648, https://doi.org/10.1155/2019/5602648.

Banfield, J.F., Barker, W.W., Welch, S.A., and Taunton, A. (1999) Biological impact on mineral dissolution: Application of the lichen model to understanding mineral weathering in the rhizosphere. Proceedings of the National Academy of Sciences of the United States of America, 96, 3404–3411, https://doi.org/10.1073/pnas.96.7.3404.

Bradford, S.Y.C., El Khoury, L., Ge, Y., Osato, M., Mobley, D.L., and Fischer, M. (2021) Temperature artifacts in protein structures bias ligand-binding predictions. Chemical Science (Cambridge), 12, 11275–11293, https://doi.org/10.1039/D1SC02751D.

Brantley, S.L. (2008) Kinetics of mineral dissolution. In S.L. Brantley, J.D. Kubicki, and A.F. White, Eds., Kinetics of Water-Rock Interaction, p. 151–210. Springer.

Bray, A.W., Oelkers, E.H., Bonneville, S., Wolff-Boenisch, D., Potts, N.J., Fones, G., and Benning, L.G. (2015) The effect of pH, grain size, and organic ligands on biotite weathering rates. Geochimica et Cosmochimica Acta, 164, 127–145, https://doi.org/10.1016/j.gca.2015.04.048.

Cao, J., Wu, X., Huang, F., Hu, B., Groves, C., Yang, H., and Zhang, C. (2018) Global significance of the carbon cycle in the karst dynamic system: Evidence from geological and ecological processes. China Geology, 1, 17–27, https://doi.org/10.31035/cg2018004.

de Souza, C.M.D., Carneiro, C.E.A., Baú, J.P.T., da Costa, A.C.S., Ivashita, F.F., Paesano, A. Jr., di Mauro, E., de Santana, H., Holm, N.G., Neubeck, A., and others. (2013) Interaction of forsterite-91 with distilled water and artificial seawater: A prebiotic chemistry experiment. International Journal of Astrobiology, 12, 135–143, https://doi.org/10.1017/S147355041200050X.

Furrer, G. and Stumm, W. (1986) The coordination chemistry of weathering: 1. Dissolution kinetics of δ-Al_2O_3 and BeO. Geochimica et Cosmochimica Acta, 50, 1847–1860, https://doi.org/10.1016/0016-7037(86)90243-7.

Gin, S., Delaye, J.-M., Angeli, F., and Schuller, S. (2021) Aqueous alteration of silicate glass: state of knowledge and perspectives. npj Materials Degradation, 5, 1–20.

Green, E. and Luttge, A. (2006) Incongruent dissolution of wollastonite measured with vertical scanning interferometry. American Mineralogist, 91, 430–434, https://doi.org/10.2138/am.2006.1968.

Hamilton, J.P., Brantley, S.L., Pantano, C.G., Criscenti, L.J., and Kubicki, J.D. (2001) Dissolution of nepheline, jadeite and albite glasses: Toward better models for aluminosilicate dissolution. Geochimica et Cosmochimica Acta, 65, 3683–3702, https://doi.org/10.1016/S0016-7037(01)00724-4.

Hänchen, M., Prigiobbe, V., Storti, G., Seward, T.M., and Mazzotti, M. (2006) Dissolution kinetics of fosteritic olivine at 90–150 °C including effects of the presence of CO_2. Geochimica et Cosmochimica Acta, 70, 4403–4416, https://doi.org/10.1016/j.gca.2006.06.1560.

Huang, W.H. and Keller, W.D. (1970) Dissolution of rock-forming silicate minerals in organic acids: Simulated first-stage weathering of fresh mineral surfaces. American Mineralogist, 55, 2076–2094.

Kahl, W.-A., Klügel, A., Bach, W., and Murshed, M. (2022) Enhanced weathering in the seabed: Rapid olivine dissolution and iron sulfide formation in submarine volcanic ash. American Mineralogist, 107, 1668–1680, https://doi.org/10.2138/am-2022-8057.

Kaszuba, J., Yardley, B., and Andreani, M. (2013) Experimental perspectives of mineral dissolution and precipitation due to carbon dioxide-water-rock interactions. Reviews in Mineralogy and Geochemistry, 77, 153–188, https://doi.org/10.2138/rmg.2013.77.5.

Khan, A., Singh, P., and Srivastava, A. (2018) Synthesis, nature and utility of universal iron chelator—Siderophore: A review. Microbiological Research, 212-213, 103–111,

https://doi.org/10.1016/j.micres.2017.10.012.
Kikuchi, S., Wang, J., Dandar, O., Uno, M., Watanabe, N., Hirano, N., and Tsuchiya, N. (2023) $NaHCO_3$ as a carrier of CO_2 and its enhancement effect on mineralization during hydrothermal alteration of basalt. Frontiers in Environmental Science, 11, 1138007, https://doi.org/10.3389/fenvs.2023.1138007.
Kołodyńska, D. (2011) Chelating Agents of a New Generation as an Alternative to Conventional Chelators for Heavy Metal Ions Removal from Different Waste Waters. Expanding Issues in Desalination. IntechOpen.
Konrad-Schmolke, M., Halama, R., Wirth, R., Thomen, A., Klitscher, N., Morales, L., Schreiber, A., and Wilke, F.D.H. (2018) Mineral dissolution and reprecipitation mediated by an amorphous phase. Nature Communications, 9, 1637, https://doi.org/10.1038/s41467-018-03944-z.
Lasaga, A.C. and Lüttge, A. (2004) Mineralogical approaches to fundamental crystal dissolution kinetics. American Mineralogist, 89, 527–540, https://doi.org/10.2138/am-2004-0407.
Li, S., Yao, J., Mou, W., Luo, A., Wang, Q., Deng, X., Chu, M., Li, Y., and Yan, C. (2018) The dissolution characteristics of the Chang 8 tight reservoir and its quantitative influence on porosity in the Jiyuan area, Ordos Basin, China. Journal of Natural Gas Geoscience, 3, 95–108, https://doi.org/10.1016/j.jnggs.2018.04.002.
Liu, Y., Olsen, A.A., and Rimstidt, J.D. (2006) Mechanism for the dissolution of olivine series minerals in acidic solutions. American Mineralogist, 91, 455–458, https://doi.org/10.2138/am.2006.2077.
Ludwig, C., Casey, W.H., and Rock, P.A. (1995) Prediction of ligand-promoted dissolution rates from the reactivities of aqueous complexes. Nature, 375, 44–47, https://doi.org/10.1038/375044a0.
Marabini, A.M., Ciriachi, M., Plescia, P., and Barbaro, M. (2007) Chelating reagents for flotation. Minerals Engineering, 20, 1014–1025, https://doi.org/10.1016/j.mineng.2007.03.012.
Martin, D.P., Blachly, P.G., Marts, A.R., Woodruff, T.M., de Oliveira, C.A.F., McCammon, J.A., Tierney, D.L., and Cohen, S.M. (2014) 'Unconventional' coordination chemistry by metal chelating fragments in a metalloprotein active site. Journal of the American Chemical Society, 136, 5400–5406, https://doi.org/10.1021/ja500616m.
Morrow, C.P., Olsen, A.A., and Kubicki, J.D. (2014) Quantum mechanical modeling of hydrolysis and H_2O-exchange in Mg-, Ca-, and Ni-silicate clusters: Implications for dissolution mechanisms of olivine minerals. American Mineralogist, 99, 2303–2312, https://doi.org/10.2138/am-2014-4635.
Neaman, A., Chorover, J., and Brantley, S.L. (2006) Effects of organic ligands on granite dissolution in batch experiments at pH 6. American Journal of Science, 306, 451–473, https://doi.org/10.2475/06.2006.03.
Newcomb, C.J., Qafoku, N.P., Grate, J.W., Bailey, V.L., and De Yoreo, J.J. (2017) Developing a molecular picture of soil organic matter-mineral interactions by quantifying organo-mineral binding. Nature Communications, 8, 396, https://doi.org/10.1038/s41467-017-00407-9.
Nowack, B. (2002) Environmental chemistry of aminopolycarboxylate chelating agents. Environmental Science & Technology, 36, 4009–4016, https://doi.org/10.1021/es025683s.
Onawole, A.T., Hussein, I.A., Saad, M.A., Mahmoud, M., Ahmed, M.E.M., and Nimir, H.I. (2019) Effect of pH on acidic and basic chelating agents used in the removal of iron sulfide scales: A computational study. Journal of Petroleum Science Engineering, 178, 649–654, https://doi.org/10.1016/j.petrol.2019.03.075.
Park, A.H.A., Jadhav, R., and Fan, L.S. (2003) CO_2 mineral sequestration: Chemically enhanced aqueous carbonation of serpentine. Canadian Journal of Chemical Engineering, 81, 885–890, https://doi.org/10.1002/cjce.5450810373.
Poulson, S.R., Drever, J.I., and Stillings, L.L. (1997) Aqueous Si-oxalate complexing, oxalate adsorption onto quartz, and the effect of oxalate upon quartz dissolution rates. Chemical Geology, 140, 1–7, https://doi.org/10.1016/S0009-2541(96)00177-5.
Prigiobbe, V., Costa, G., Baciocchi, R., Hänchen, M., and Mazzotti, M. (2009) The effect of CO_2 and salinity on olivine dissolution kinetics at 120 °C. Chemical Engineering Science, 64, 3510–3515, https://doi.org/10.1016/j.ces.2009.04.035.
Putnis, A. (2014) Why mineral interfaces matter. Science, 343, 1441–1442, https://doi.org/10.1126/science.1250884.
Putnis, A., Junta-Rosso, J.L., and Hochella, M.F. Jr. (1995) Dissolution of barite by a chelating ligand: An atomic force microscopy study. Geochimica et Cosmochimica Acta, 59, 4623–4632, https://doi.org/10.1016/0016-7037(95)00324-X.
Ribeiro, I.D.A., Volpiano, C.G., Vargas, L.K., Granada, C.E., Lisboa, B.B., and Passaglia, L.M.P. (2020) Use of mineral weathering bacteria to enhance nutrient availability in crops: A review. Frontiers in Plant Science, 11, 590774, https://doi.org/10.3389/fpls.2020.590774.
Seyama, H. and Soma, M. (1985) Bonding-state characterization of the constitutent elements of silicate minerals by X-ray photoelectron spectroscopy. Journal of the Chemical Society, Faraday Transactions 1, 81, 485–495, https://doi.org/10.1039/F19858100485.
Stumm, W. (1997) Reactivity at the mineral-water interface: Dissolution and inhibition. Colloids and Surfaces A, Physicochemical and Engineering Aspects, 120, 143–166, https://doi.org/10.1016/S0927-7757(96)03866-6.
Stumm, W. and Wollast, R. (1990) Coordination chemistry of weathering: Kinetics of the surface-controlled dissolution of oxide minerals. Reviews of Geophysics, 28, 53–69, https://doi.org/10.1029/RG028i001p00053.
Takahashi, R., Wang, J., and Watanabe, N. (2023) Process and optimum pH for permeability enhancement of fractured granite through selective mineral dissolution by chelating agent flooding. Geothermics, 109, 102646, https://doi.org/10.1016/j.geothermics.2022.102646.
Torres, M.A., Dong, S., Nealson, K.H., and West, A.J. (2019) The kinetics of siderophore-mediated olivine dissolution. Geobiology, 17, 401–416, https://doi.org/10.1111/gbi.12332.
Walter, M., Schenkeveld, W.D.C., Reissner, M., Gille, L., and Kraemer, S.M. (2019) The effect of pH and biogenic ligands on the weathering of chrysotile asbestos: The pivotal role of tetrahedral Fe in dissolution kinetics and radical formation. Chemistry (Weinheim an der Bergstrasse, Germany), 25, 3286–3300, https://doi.org/10.1002/chem.201804319.
Wang, J., Watanabe, N., Okamoto, A., Nakamura, K., and Komai, T. (2019) Enhanced hydrogen production with carbon storage by olivine alteration in CO_2-rich hydrothermal environments. Journal of CO2 Utilization, 30, 205–213.
Wang, J., Watanabe, N., Inomoto, K., Kamitakahara, M., Nakamura, K., Komai, T., and Tsuchiya, N. (2021) Enhancement of aragonite mineralization with a chelating agent for CO_2 storage and utilization at low to moderate temperatures. Scientific Reports, 11, 13956, https://doi.org/10.1038/s41598-021-93550-9.
——— (2022) Sustainable process for enhanced CO_2 mineralization of calcium silicates using a recyclable chelating agent under alkaline conditions. Journal of Environmental Chemical Engineering, 10, 107055, https://doi.org/10.1016/j.jece.2021.107055.
Watanabe, N., Takahashi, K., Takahashi, R., Nakamura, K., Kumano, Y., Akaku, K., Tamagawa, T., and Komai, T. (2021) Novel chemical stimulation for geothermal reservoirs by chelating agent driven selective mineral dissolution in fractured rocks. Scientific Reports, 11, 19994, https://doi.org/10.1038/s41598-021-99511-6.
Wogelius, R.A. and Walther, J.V. (1992) Olivine dissolution kinetics at near-surface conditions. Chemical Geology, 97, 101–112, https://doi.org/10.1016/0009-2541(92)90138-U.
Xiong, Y., Yao, S., Inoue, S., Epping, J.D., and Driess, M. (2013) A cyclic silylone ("siladicarbene") with an electron-rich silicon(0) atom. Angewandte Chemie International Edition, 52, 7147–7150, https://doi.org/10.1002/anie.201302537.
Xu, R., Li, R., Ma, J., He, D., and Jiang, P. (2017) Effect of mineral dissolution/precipitation and CO_2 exsolution on CO_2 transport in geological carbon storage. Accounts of Chemical Research, 50, 2056–2066, https://doi.org/10.1021/acs.accounts.6b00651.
Yadav, S.K. and Chakrapani, G.J. (2006) Dissolution kinetics of rock-water interactions and its implications. Current Science, 90, 932–937.
Zhu, J., Tang, C., Wei, J., Li, Z., Laipan, M., He, H., Liang, X., Tao, Q., and Cai, L. (2018) Structural effects on dissolution of silica polymorphs in various solutions. Inorganica Chimica Acta, 471, 57–65, https://doi.org/10.1016/j.ica.2017.10.003.

Manuscript received April 13, 2023
Manuscript accepted December 23, 2023
Accepted manuscript online January 2, 2024
Manuscript handled by Di Wu